Search for a heavy di-photon resonance in association with b-jets with the ATLAS detector at the LHC

E. Shrif[1], X. Ruan[1], S. Dahbi[1] and B. Mellado[1,2]

[1] School of Physics and Institute for Collider Particle Physics, University of the Witwatersrand, Johannesburg, Wits 2050, South Africa

[2] iThemba LABS, National Research Foundation, PO Box 722, Somerset West 7129, South Africa

E-mail: shrif.esra@gmail.com

Abstract. A search for a heavy resonance decaying into di-photon in association with at least one b-jet in the mass range, 180–1600 GeV is performed using 139 fb^{-1} of $\sqrt{s} = 13$ TeV pp collision data taken by the ATLAS detector at the Large Hadron Collider. A Higgs boson like heavy scalar X produced with top quarks, b quarks or Z boson decaying into $b\bar{b}$ are examined. Three models are tested in this search. Limits at 95% confidence level on the production cross-section times branching fraction to di-photon are set.

1. Introduction

Many proposals for theories beyond the Standard Model (SM), include the prediction of new massive bosons. Examples are, the graviton models [1] and the two-Higgs-doublet models (2HDM) [2], that address the large difference between the electroweak and gravitational scales. It is therefore well-motivated to extend the upper limit of the Higgs boson search mass range as much as possible above $m_H = 160$ GeV. The analyses presented here search for a heavy resonance decaying into two photons and produced in association with at least a b quark. Similar analyses have been performed by ATLAS [3] and CMS [4] in the $\mu^+\mu^-$ and $b\bar{b}$ final states. Three production modes are tested in this search, the $t\bar{t}X$, $b\bar{b}X$ and the ZX, where the Z boson decays into two b quarks, and X is assumed to be a Higgs like heavy resonance. The Feynman diagrams for these modes are shown in Fig. 1. The search examines the diphoton invariant mass spectrum from 130 GeV to 1.6 TeV with one b tagged jet, two b tagged jets and one b tagged jet plus one lepton final states. This analysis uses 139 fb^{-1} data taken from ATLAS experiment during 2015–2018 with the centre of mass energy at 13 TeV. Limits at 95% confidence level (CLs) on the production cross-section times branching ratio to diphoton final state are set on the resonance range from 180 GeV to 1.6 TeV. Only the narrow width assumption is tested.
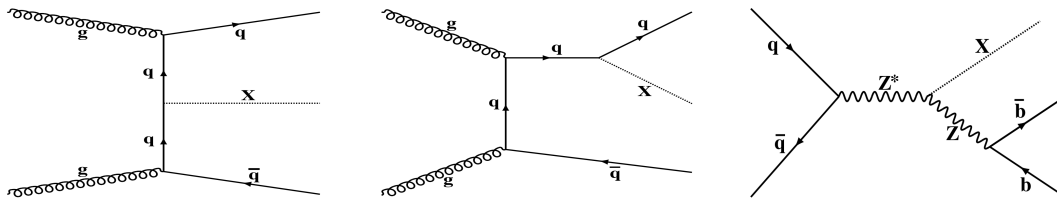

Figure 1: Feynman diagrams for the signal processes, with q refers to top or bottom quark.
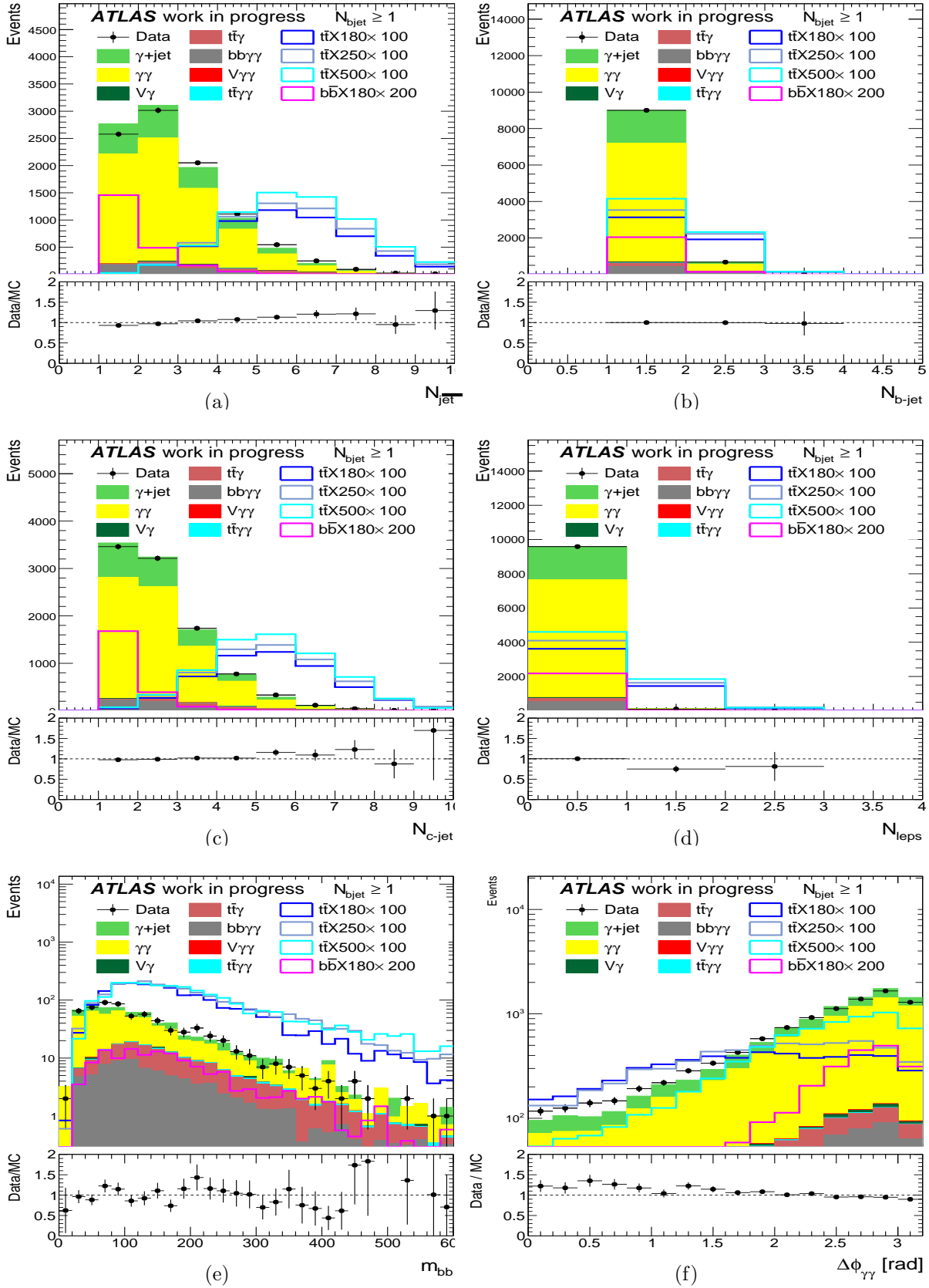
Figure 2: Kinematic distributions comparing the data to MC (after pre-selection and in the control region that $130 < m_{\gamma\gamma} < 160\,[\text{GeV}]$). The multiplicity of jet (a), b-jet (b) and central jet (c). Number of leptons (d), the invariant mass of the two leading b-jets (e) and $\Delta\phi(\gamma\gamma)$ (f).

2. Samples and event pre-selection

Signal and background samples are simulated using Monte Carlo (MC) generators according to ATLAS detector configurations. MADGRAPH [5] generator, at next-to-leading order in QCD, is used to produce the $t\bar{t}X$ signal samples. Parton showering and hadronization are simulated using the PYTHIA8 [6]. The $t\bar{t}X$ and ZX signals samples are generated and showered using PYTHIA8 at leading order in QCD. The dominant background samples used here are the SM diphoton production and γ jet; contributions also come from $V\gamma$, $V\gamma\gamma$, $t\bar{t}\gamma\gamma$, $t\bar{t}\gamma$ and $b\bar{b}\gamma\gamma$, where V stands for Z or W boson. The dataset used in this analysis encompasses all data that was recorded with the ATLAS detector, between 2015 and 2018, in pp collisions with an integrated luminosity of 140 fb^{-1} at a centre-of-mass energy of $\sqrt{s} = 13$ TeV.

In the pre-selections, events are selected with two identified and isolated photons invariant mass $m_{\gamma\gamma} > 130$ GeV. The transverse momentum p_T of the leading and sub-leading photon are required to be greater than 40 GeV, and 30 GeV, respectively. Events should also have at least one b-tagged jets. The working point chosen is set at 77% b-tagged jet selection efficiency [7]. Figure 2 shows the kinematic distributions corresponding to different variables, just after the pre-selections. The agreement between data and total background is reasonable within the statistical uncertainties.

3. Optimization

The optimization is performed based on the pre-selection, We use the $t\bar{t}X$ sample with $m_X = 180$ GeV, $b\bar{b}X$ with $m_X = 180$ GeV and ZX with $m_X = 200$ GeV as the signal sample for optimization. All background samples are mixed and normalised to 140 fb^{-1} for the optimization. For $t\bar{t}X$, we chose to optimize on the variables N_{cjet} and $\Delta\phi_{\gamma\gamma}$ due to the best performance comparing to other variables, like missing transverse momentum and transverse momentum of the two photon system. Events are split into three regions, namely, leptonic ($N_{leps} \geq 1$ and $N_{bjet} \geq 1$), Zero leptons with exactly one b-tagged jet or at least two b-tagged jet. In each region, events are further split into four bins by making a two dimension scan on $\Delta\phi_{\gamma\gamma}$ and N_{cjet}. For the ZX model, we optimize using the variable m_{bb} and $\Delta\phi_{\gamma\gamma}$ in the two b-jet region, where m_{bb} is the invariant mass of the two leading b-jets. While we only use the number of central jets for the $b\bar{b}X$ optimization. The significance is calculated using the formula $S/\sqrt{B}$, where S and B are the signal and background events, respectively. Table 1 shows a summary of the optimized results for $t\bar{t}X$ and ZX models. Based on these optimization results as well as the $b\bar{b}X$ results, the events are categorized in Table 2.

Table 1: The optimization results for the $t\bar{t}X$ model with $m_X = 180, 250$ GeV for each region (left) and for the ZX model with $m_X = 200$ GeV in the two b-jet region (right).

	Region	N_{Cjet}	$\Delta\phi(\gamma\gamma)$	Significance
	$1l1b$	3	1.2	2.75
ttX180	$0l1b$	6	2.4	1.26
	$0l2b$	5	2.0	1.80
	$1l1b$	6	1.2	5.94
ttX250	$0l1b$	6	2.0	2.00
	$0l2b$	6	2.4	3.18

	$ZX200$		
$\Delta\phi(\gamma\gamma)$	m_{bb}(high)	m_{bb}(low)	Significance
1.6	105	65	0.284
2.0	105	65	0.289
2.4	105	65	0.294
2.8	105	70	0.281
3.2	105	65	0.262

Table 2: The definition of each category, for different models and mass range.

	Category index	Cuts
Preselection		Photon $m_{\gamma\gamma} > 130$ GeV & $p_T > 40, 30$ GeV & $N_{bjet} \geq 1$
$m_{\gamma\gamma}$ in 160-1600 GeV		
$b\bar{b}X$ Categories	1	$N_{cj} = 1$
	2	$N_{cj} \geq 2$
$m_{\gamma\gamma}$ in 160-600 GeV		
$t\bar{t}X$ Categories	3	$N_{bj} \geq 1$ & $N_{leps} \geq 1$ & $N_{cj} >= 4$
	4	$N_{bj} \geq 1$ & $N_{leps} \geq 1$ & $N_{cj} < 4$
	5	$N_{bj} \geq 2$ & $N_{leps} = 0$ & $N_{cj} \geq 5$ & $\Delta\phi_{\gamma\gamma} < 2$
	6	$N_{bj} \geq 2$ & $N_{leps} = 0$ & $N_{cj} \geq 5$ & $\Delta\phi_{\gamma\gamma} > 2$
	7	$N_{bj} \geq 2$ & $N_{leps} = 0$ & $N_{cj} < 5$
	8	$N_{bj} = 1$ & $N_{leps} = 0$ & $N_{cj} \geq 6$ & $\Delta\phi_{\gamma\gamma} < 2.4$
	9	$N_{bj} = 1$ & $N_{leps} = 0$ & $N_{cj} \geq 6$ & $\Delta\phi_{\gamma\gamma} > 2.4$
	10	$N_{bj} = 1$ & $N_{leps} = 0$ & $N_{cj} < 6$
ZX Categories	11	$N_{bj} \geq 2$ & $m_{bb} > 65$ & $m_{bb} < 105$ & $\Delta\phi_{\gamma\gamma} < 2.4$
	12	$N_{bj} \geq 2$ & $m_{bb} > 65$ & $m_{bb} < 105$ & $\Delta\phi_{\gamma\gamma} > 2.4$
	13	$N_{bj} \geq 2$ & $(m_{bb} < 65$ & $m_{bb} > 105)$
	14	$N_{bj} = 1$
$t\bar{t}X$, ZX for $m_{\gamma\gamma}$ in 600-900 GeV		
	14	$N_{bj} = 1$
	15	$N_{bj} \geq 2$
$t\bar{t}X$, ZX for $m_{\gamma\gamma}$ in 900-1600 GeV		
	0	$N_{bjet} \geq 1$

4. Signal and background modelling

To model the heavy scalar signal shape, we use a functional form that is the double-sided Crystal Ball function (DSCB) [8], consisting of a Gaussian central part extended by asymmetric power-law tails on both sides. The DSCB function modelling method is described in detail in [9, 10]. The DSCB shape is fitted to the signal distributions of the di-photon invariant mass spectrum for different mass points m_X, yielding a set of DSCB parameters for each category. As an example, Figure 4a, shows the result of a single fit of the DSCB function (lines) for a $t\bar{t}X$ signal sample with mass point $m_X = 180$ GeV for the category 3. The DSCB parameter σ_{CB}, the width of the Gaussian core (representing the detector resolution) and α are then parametrised as a function of m_X for each process for the all categorizes using linear functions. For instance, Figure 4b shows σ_{CB} for the $t\bar{t}X$ category 3 with all the signal mass points, where σ_{CB} increases for the signals at higher mass points. For simplicity, the ns for each model are set to the fixed value.

To estimate the signal yield, we parameterize the acceptance times efficiencies using a variety of analytic functions (linear, exponential functions of different-order or polynomials). The maximum difference between the predicted acceptance times efficiency and the MC points is treated as the systematic uncertainty. We only use the maximum difference within the mass range where the category is used. For example, we only use the maximum difference below $m_X = 700$ GeV for category 3-13. The statistical uncertainty of the MC samples is also taken into account.

To build up the background model, the diphoton purity is estimated by the 2×2D sideband method with at least one b-jet selection. The method uses the information of photon ID and
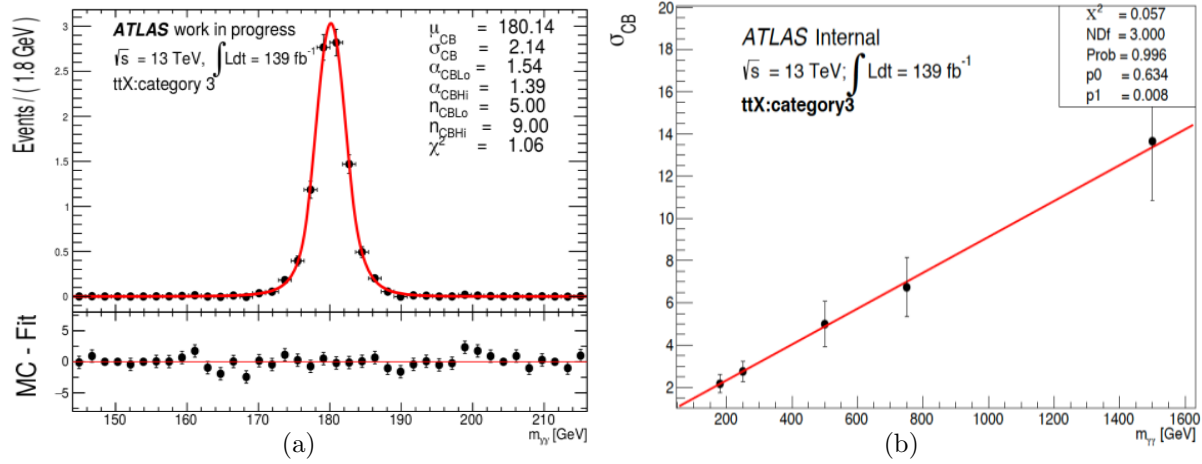
Figure 3: (a) Fit of the $m_{\gamma\gamma}$ for $t\bar{t}X$ with $m_X = 180$ GeV to a DSCB in category–3 and (b) Resolution of the resonance peak as a function $m_{\gamma\gamma}$ for $t\bar{t}X$ in category–3.

isolation variables to measure the fraction of the diphoton events from the data. More details of the method are found in Ref. [11]. The $\gamma\gamma$ and γ jet purity is estimated, and the measured purity is shown in Table 3. The uncertainty on the background modelling is parameterized using so called spurious signal. There are several functional forms to describe the background shape in large mass range. They are the different orders of the so called Dijet fit functions [12]: $f_k(x; b, \{a_k\}) = (1 - x)^b x^{\sum_{j=0}^{k} a_j \log(x)^j}$, $k = 0, 1, 2$, noted as FK0, FK1 and FK2. The envelops of the absolute spurious signals are obtained in each category. They are parametrised between 160-1500 GeV with a second polynomial exponential function with a constant term, as Figure 4 shows. F–test is used to decide which functional form to be used in each category. For instance, the function FK2 is selected for cateory–0.

Table 3: Purities with 2×2D sideband method with at least one b-jet selection.

	$\gamma - jet, jet - \gamma$ fraction	jet–jet fraction	$\gamma\gamma$ purity
$m_{\gamma\gamma} > 130$ GeV	0.18 ± 0.01	0.02 ± 0.00	0.80 ± 0.01
180 GeV $< m_{\gamma\gamma} < 700$ GeV	0.20 ± 0.01	0.02 ± 0.00	0.78 ± 0.01
$m_{\gamma\gamma} > 700$ GeV	0.15 ± 0.06	0.02 ± 0.02	0.83 ± 0.07

5. Uncertainties and results

Both the experimental and theoretical uncertainties are used in obtaining the result of this analysis. As the background shapes are described by fitting in the data, the uncertainties except the spurious signal, which is discussed as previous section, are estimated on the signal samples only. The systematic uncertainties are implemented via nuisance parameters in the profiled likelihood fit. A summary of the experimental and theoretical uncertainties is given in Table 4 in terms of the relative impact on the number of events from the signal for the most sensitive category. The fits are performed on each mass points for each model. The CLs limits on the production cross-section times the branching fraction $X \to \gamma\gamma$ are set to each of the model as a function of mass, as shown in Figure 5.
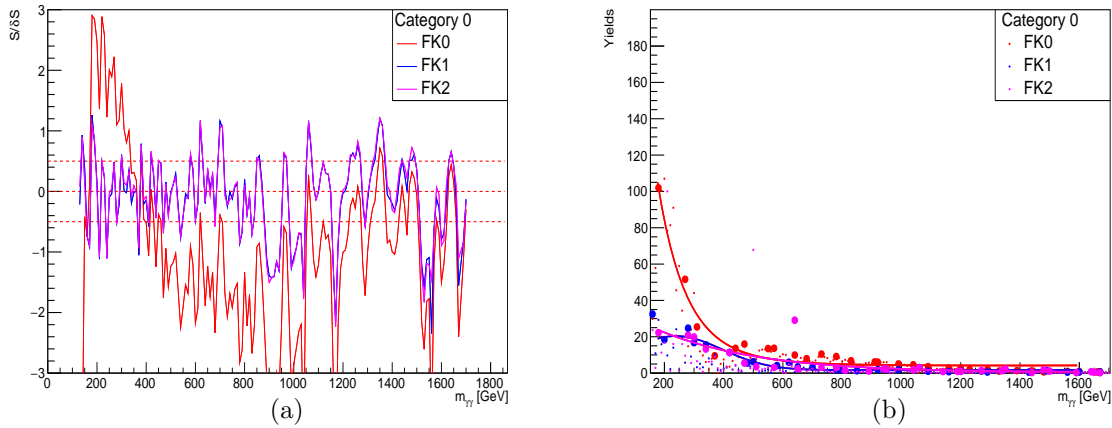
Figure 4: (a) The N_{spurious} envelop for each functional form for the $t\bar{t}X$ category 1 and (b) The $N_{\text{spurious}}/\delta N_{\text{spurious}}$ as a function of mass for each functional using background in category–1.

Table 4: Summary of the systematic uncertainties.

	Source	Signal uncertainty (%)
Experimental	Luminosity	1.7
	Trigger efficiency	1.0
	Vertex selection (inclusive cat.)	< 0.01
	Photon identification efficiency	0.6–1.5
	Photon identification efficiency due to fast simulation	2.0
	Photon isolation efficiency	0.6–1.5
	Photon energy resolution	0.6
	Pile-up reweighting	2.0–7.4
	Photon energy scale	0.3
	Signal efficiency interpolation	1.3–9
Theoretical	Factorization and renormalization scale in migration	1–7
	PDF+α_S in migration	1–5
	PS, hadronization	3.0
	ISR, FSR, Multi-parton interactions	3.0–10.0

6. Summary

An analysis to search for new heavy resonance in di-photon channel is presented. Three models are tested in this search: $t\bar{t}X$, $b\bar{b}X$ and ZX. The expected 95% confidence level limits are set on the production cross-section times the branching fraction for the decay of the resonance into di-photon as a function of m_X. The mass range of the hypothetical resonances considered is between 180 GeV and 1.6 TeV depending on the final state the model considered.
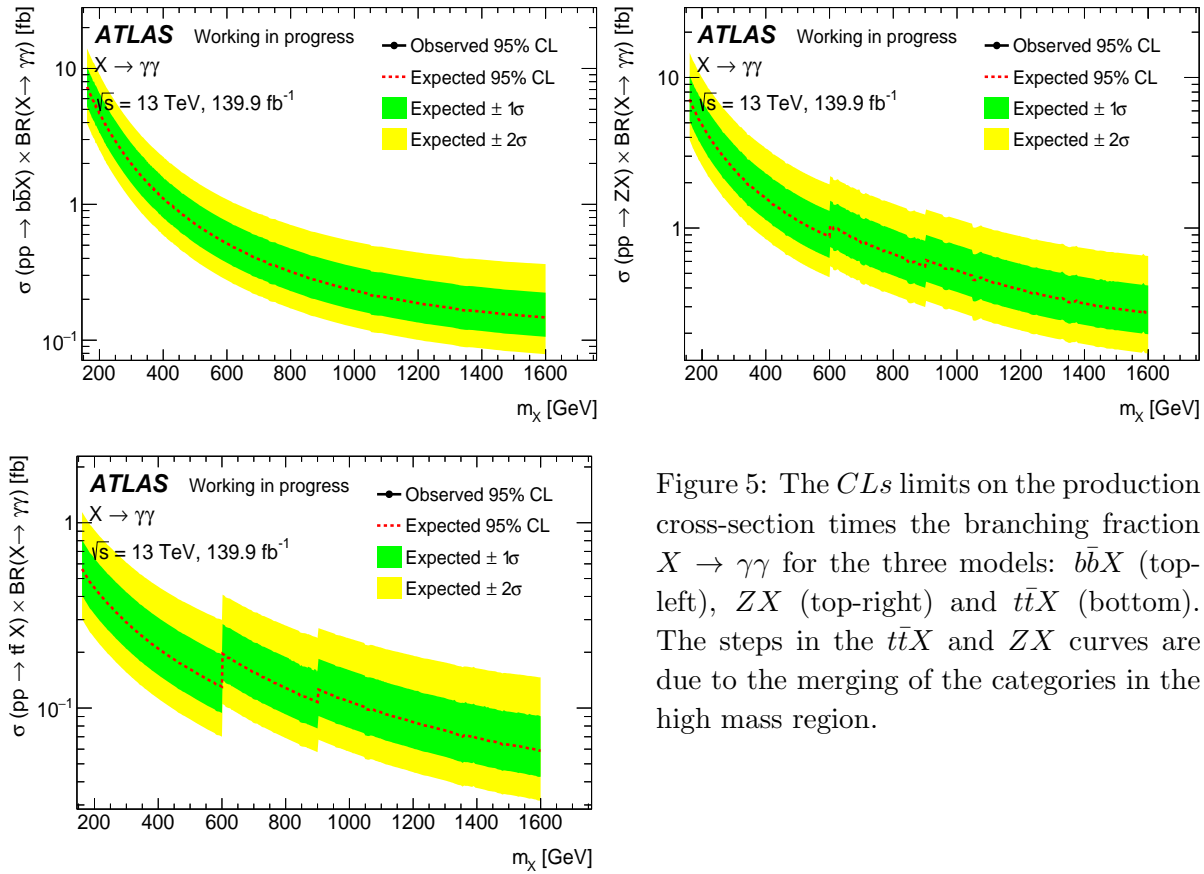
Figure 5: The CLs limits on the production cross-section times the branching fraction $X \to \gamma\gamma$ for the three models: $b\bar{b}X$ (top-left), ZX (top-right) and $t\bar{t}X$ (bottom). The steps in the $t\bar{t}X$ and ZX curves are due to the merging of the categories in the high mass region.

References

[1] H. Davoudiasl, J. L. Hewett and T. G. Rizzo, (2000) Phys. Rev. Lett. **84**, 2080.

[2] G. C. Branco, P. M. Ferreira, L. Lavoura, M. N. Rebelo, M. Sher and J. P. Silva, Phys. Rept. **516**, 1-102 (2012) [arXiv:1106.0034].

[3] ATLAS Collaboration, JHEP **07**, 117 (2019) [arXiv:1901.08144].

[4] CMS Collaboration, JHEP **08**, 113 (2018) [arXiv:1805.12191].

[5] Alwall J, Frederix R, Frixione S, Hirschi V, Maltoni F, Mattelaer O, Shao H S, Stelzer T, Torrielli P and Zaro M, JHEP 1407, 079 (2014) [arXiv:1405.0301].

[6] Sjostrand T, Mrenna S and Skands P Z, Comput. Phys. Commun. 178, 852 (2008) [arXiv:0710.3820].

[7] ATLAS Collaboration, (2017) [ATL-PHYS-PUB-2017-013].

[8] Oreglia M, Appendix D. PhDthesis, Univ. Stanford, [SLAC-0236 (1980)].

[9] ATLAS Collaboration, Phys. Rev. D **90**, no.11, 112015 (2014) [arXiv:1408.7084].

[10] ATLAS Collaboration, JHEP **09**, 001 (2016) [arXiv:1606.03833].

[11] Carminati L *et al.* (2012) [ATL-COM-PHYS-2012-592].

[12] CDF Collaboration, Phys. Rev. D **79**, 112002 (2009) [arXiv:0812.4036].